Drying Technology
An International Journal

ISSN: (Print) (Online) Journal homepage: https://www.tandfonline.com/loi/ldrt20

Application of experimental, numerical, and machine learning methods to improve drying performance and decrease energy consumption of tunnel-type food dryer

Murat Catalkaya, O. Erdal Akay, Mehmet Das & Ebru Akpinar

To cite this article: Murat Catalkaya, O. Erdal Akay, Mehmet Das & Ebru Akpinar (2023): Application of experimental, numerical, and machine learning methods to improve drying performance and decrease energy consumption of tunnel-type food dryer, Drying Technology, DOI: 10.1080/07373937.2023.2216781

To link to this article: https://doi.org/10.1080/07373937.2023.2216781

Published online: 08 Jun 2023.

DRYING TECHNOLOGY
https://doi.org/10.1080/07373937.2023.2216781

Application of experimental, numerical, and machine learning methods to improve drying performance and decrease energy consumption of tunnel-type food dryer

Murat Catalkaya[a], O. Erdal Akay[a], Mehmet Das[b], and Ebru Akpinar[c]

[a]Mechanical Engineering Department, Kahramanmaraş Sütçüimam University, Kahramanmaraş, Turkey; [b]Mechatronic Engineering Department, Engineering Faculty, Firat University, Elazig, Turkey; [c]Mechanical Engineering Department, Engineering Faculty, Firat University, Elazig, Turkey

ABSTRACT

In this study, to distribute the drying air uniformly on the product surface, straight and trapeze air barriers were designed in the drying chamber of the existing tunnel dryer. The effects of air barriers on product surface temperature changes were investigated by computational fluid dynamics analysis (CFD). Drying time in the experiment without an air barrier decreased by 45% with the trapeze barrier and 20% with the straight barrier. Likewise, the trapeze barrier provided 53.9% energy savings, and the straight barrier 37.4% energy saving compared to the drying process carried out in the current system. Also, using the experimental data, mathematical equations that can calculate activation energy (E_a) in the drying process were produced with the help of regression-based artificial intelligence methods (Pace and Elastic.Net). With the help of these equations, the E_a values of the drying process performed under different experimental conditions were determined, and a 1.03% error value was calculated between the obtained E_a values and the experimental values.

ARTICLE HISTORY
Received 21 March 2023
Revised 13 May 2023
Accepted 16 May 2023

KEYWORDS
Tunnel dryer; convective heat transfer coefficient; activation energy; CFD; Pace regression; Elastic.Net regression

1. Introduction

Fresh vegetables and fruits can spoil quickly due to their high moisture content. Thanks to drying, the moisture content can be reduced to low levels and the storage period of the product can be extended. This prevents the formation of microorganisms in the product.[1] Today, energy-efficient long-term food use methods have become increasingly important after significant crises such as energy and food supply problems.[2] Solar systems are widely used in food drying.[3,4] Although the product drying process is based on renewable energy in these systems, the drying times are pretty long. Since solar energy is not continuous, complete drying of the food product does not occur, and the amount of water in the product does not decrease over a continuous period. This situation prolongs the drying process and adversely affects the quality of the product. For these reasons, as an alternative to solar energy systems, tunnel-type or shelf-type drying systems are used for fast and high-quality drying of products.[5–7] Since the continuous drying process is carried out in tunnel-type dryers, the drying rate of the product is relatively high. Electricity is generally used as the energy source in tunnel dryers. The generation of hot air with resistance heaters increases electrical energy consumption. In order to provide lower energy consumption, different system designs are made in tunnel-type dryers. These designs are usually made by computational fluid dynamics (CFD) analysis. Turgut et al.[8] investigated potato product drying behavior in tunnel dryers at different temperatures and air velocities with the help of CFD analysis and compared the results with experimental data. With the use of CFD analysis, they observed beforehand the drying behavior of the product. Amanlou and Zomorodian[9] conducted CFD temperature and velocity distribution analyses for seven different drying cabinet types to achieve more efficient drying in the cabinet dryer. They determined the most effective drying chamber geometry through these analyses. They compared the CFD analysis results with the experimental results. Guangbin et al.[10] performed CFD analyses to determine the drying characteristics of forage seeds in the tray in a cabinet-type 10-tray dryer. They compared the experimental results with the CFD simulation results they

CONTACT Mehmet Das m.das@firat.edu.tr Mechatronic Engineering Department, Engineering Faculty, Firat University, 23279 Elazig, Turkey

obtained. With the help of these analyses, they determined which tray had the most effective temperature and air velocity distribution. Babu et al.[11] have designed a cabinet tray dryer with four different geometries for thin-layer product drying. They used the CFD analysis to examine the designed dryers' air temperature and velocity distributions. Olejnik et al.[12] determined the uneven air distribution in the cabinet dryer by CFD analysis. They obtained two different designs for uniform air distribution in the dryer, and they observed the air distribution results of these designs with the help of CFD analysis. Darabi et al.[13] made two geometric designs to achieve uniform moisture distribution in the cabinet in the cabinet-type dryer compartment. In these designs, they examined velocity and moisture distributions under various experimental conditions with the help of CFD analysis. Razavizadeh et al.[14] dried the rice product in a laboratory bed dryer and investigated the air velocity distribution of the dryer under different experimental conditions with CFD analysis. Among the different air chamber duct structures, they determined the most effective duct type with the help of CFD analysis. Ju et al.[15] expressed the temperature and moisture distributions during the drying process of papaya slices in a convective hot air dryer based on 3D simulation.

When CFD studies for tunnel-cabin-type dryers were examined in the literature, more uniform air distribution was provided as a result of the designs, appropriate drying zone selection was realized, and the optimum product drying tray geometry in the drying system was determined. However, there was no experimental or numerical study on the application of air barriers in tunnel-type drying systems. In addition, no CFD study predicts that the energy consumption value could be reduced with the design of air barriers. To fill this gap in the literature, the green capia pepper drying process was carried out in this study. For this drying process to consume less energy and have higher drying performance, two different air barrier geometries were designed with the help of CFD analysis, and the most effective barrier geometry was determined. Then, the air barriers examined with CFD were manufactured, and their effects on the drying process under different experimental conditions were investigated. Low energy consumption values and increased product drying performance were obtained compared to the pre-design. The motivation of this study is to show the beneficial changes in energy consumption and product drying performance of tunnel dryers by simple designs obtained by CFD analysis.

In the literature, in addition to CFD studies for the more effective operation of tunnel dryers, many artificial intelligence studies have been carried out to determine the behavior of different parameters in tunnel drying processes in advance. Many drying parameters have been modeled using machine learning methods in the literature, and valuable information has been obtained thanks to these models. Liu et al.[16] investigated the color changes of mushroom slices at different air velocities (3, 6, 9, and 12 m/s) and temperatures (55, 60, 65, 70, and 75 °C). They used machine learning-based Extreme Learning Machine (ELM), integrated Bayes method (BELM), and traditional Back-Propagation Neural Network (BPNN) models to predict the color changes of mushroom slices during the drying process. In the simulation results, root mean square error (RMSE) values for the accuracy of the predictions were obtained as 0.059, 0.0688, and 0.0961 for BELM, ELM, and BPNN, respectively. As a result of the study, BELM performed better than BPNN and ELM. Batuwatta-Gamage[17] developed a Physics Informed Neural Network-based artificial network framework to predict Moisture Concentration (MC) with Fick's law of diffusion and to predict Shrinkage (S) with the "free shrinkage" hypothesis. They estimated the MC and S values with an average accuracy of 81%. Kaveh et al.[18] developed a neuro-fuzzy inference system (ANFIS) and Artificial Neural Networks (ANN) model to predict the effective moisture diffusion (D_{eff}) and specific energy consumption (SEC) values of potato, garlic, and melon. They successfully estimated the D_{eff} (MSE = 0.0074) and SEC (MSE = 0.0057) values. Meerasri and Sothornvit[19] used multiple linear regression (MLR) and artificial neural networks (ANN) to predict moisture ratio (MR) and drying rate (DR) during the drying process of pineapple products. The error value of the MR values predictive model was calculated as 0.6865 RMSE and the DR as 0.8179 RMSE. Liu et al.[20] dried kiwifruit slices at different temperatures and pressure values in a pulsed vacuum dryer. They used a multilayer feed-forward neural network (MLFNN) to predict the optimum drying conditions. They used the ANN network of three inputs (drying temperature, vacuum pressure duration, and ambient pressure duration), one hidden layer, and one output (comprehensive score). With the help of ANN, they obtained the optimal drying condition at 65 °C, 12 min VPD, and 2 min APD, which obtained the highest comprehensive score for dried kiwi slices. Karaağaç et al.[21] used machine learning algorithms ANN and support vector machine (SVM) to predict

mushroom products' MC and MR values in a photovoltaic-thermal solar dryer. The RMSE values of the MC and MR predictive models were calculated as 0.033 and 0.039, respectively. Kartal and Özveren[22] used an artificial neural network model to estimate the activation energy (E_a), an essential parameter for thermochemical processes. The ANN model they obtained estimated E_a values with a mean absolute percentage error (MAPE) value of 0.02. Fabani et al.[23] used ANN to estimate the moisture content of the watermelon pulp during the drying process. They estimated the MR parameter in the drying experiments at 70 °C with the help of ANN with an error value of 0.026 RMSE. Massei et al.[24] used machine learning to estimate freeze-dried products' Residue Moisture (RM) value. They used the linear regression (LR) model and ANN as machine learning methods. They modeled the RM values with the help of the LR method with an average RMSE error value of 0.375 and with the help of the ANN method with an RMSE error value of 0.352. Liu et al.[25] dried mushroom slices at different temperatures and air velocities in a closed-cycle hot air impingement dryer and calculated the energy-exergy efficiency values of the drying processes. They used an artificial neural network to model the energy and exergy values in the drying process. Their network includes four inputs (drying time, air temperature, air velocity, and sample thickness), one hidden layer, and four outputs (energy absorption, energy utilization rate, exergy loss, and exergy efficiency). Using the ANN network structure, they obtained highly accurate predictive energy and exergy models.

Models made for convective-type dryers using various artificial intelligence methods (machine learning algorithms) in the literature are generally parametric. With these methods, which are label-based modeling, a parameter with a numerical value (energy, exergy, moisture content, effective moisture diffusion, moisture ratio, activation energy) is modeled, and a numerical value is obtained. The originality of this study, which is different from the artificial intelligence models for convective-type dryers in the literature, is that it provides a method that can generate a mathematical equation to calculate the output parameter of the input parameters used to create the model. With the help of this equation, the parameter to be modeled can be easily calculated. The study's novelty is that a mathematical equation is generated using a regression-based artificial intelligence method (Pace regression and Elastic.Net regression) to calculate the drying process's activation energy value in a tunnel dryer. Elastic.net and pace regression methods, which are different from classical regressions and define the relationship between one or more independent variables by blending ordinary least squares (OLS) and Empirical Bayes (EB) methods[26] were used to generate these equations.

2. Material and methods

In this study, experiments were carried out at constant air velocities and temperatures. The experiments were conducted to examine the drying parameters of the products carried out in the existing experimental setup and to observe the results of the modification studies that would increase the system performance. CFD analyses were also conducted to watch the effects and design of the airflow barriers used to improve the system's performance. The flow chart of the present study is shown in Figure 1.

In the experimental setup, two different drying experiments were carried out. Experiment 1 was carried out with the present experimental setup. This study was conducted to examine both the moisture content (MC), rate (MR), drying efficiency (η_d), and convective heat transfer coefficient (h_c) parameters, as well as to determine the energy consumption and drying time of the existing system. In Experiment 2, trapeze and straight air barriers determined as a result of CFD analyses were placed in the current experimental setup to reduce the system's energy consumption and the product drying time.

2.1. Experimental setup and procedure

The experimental setup used in this study is shown in Figure 2. The experimental design; consists of a tunnel-type dryer (TTD) system with dimensions of $1800 \times 200 \times 200$ mm. This system consists of a lamella electric heater for heating, one axial fan for air circulation, four sensors (T-RH%) for humidity and temperature measurement, two sensors for measuring the indoor and outdoor temperature of the dried product, one sensor for measuring air velocity, one weight sensor for monitoring the weight change of the product, and one air corrector for regulating the airflow in the tunnel (Figure 2).

Air enters the system; first, it passes through the air velocity, humidity, and temperature sensors, comes to the heater section, and is heated to the drying temperature. Later, the air passes through the straightener and humidity-temperature sensors and reaches where heat and mass transfer occur at this section's exit. It

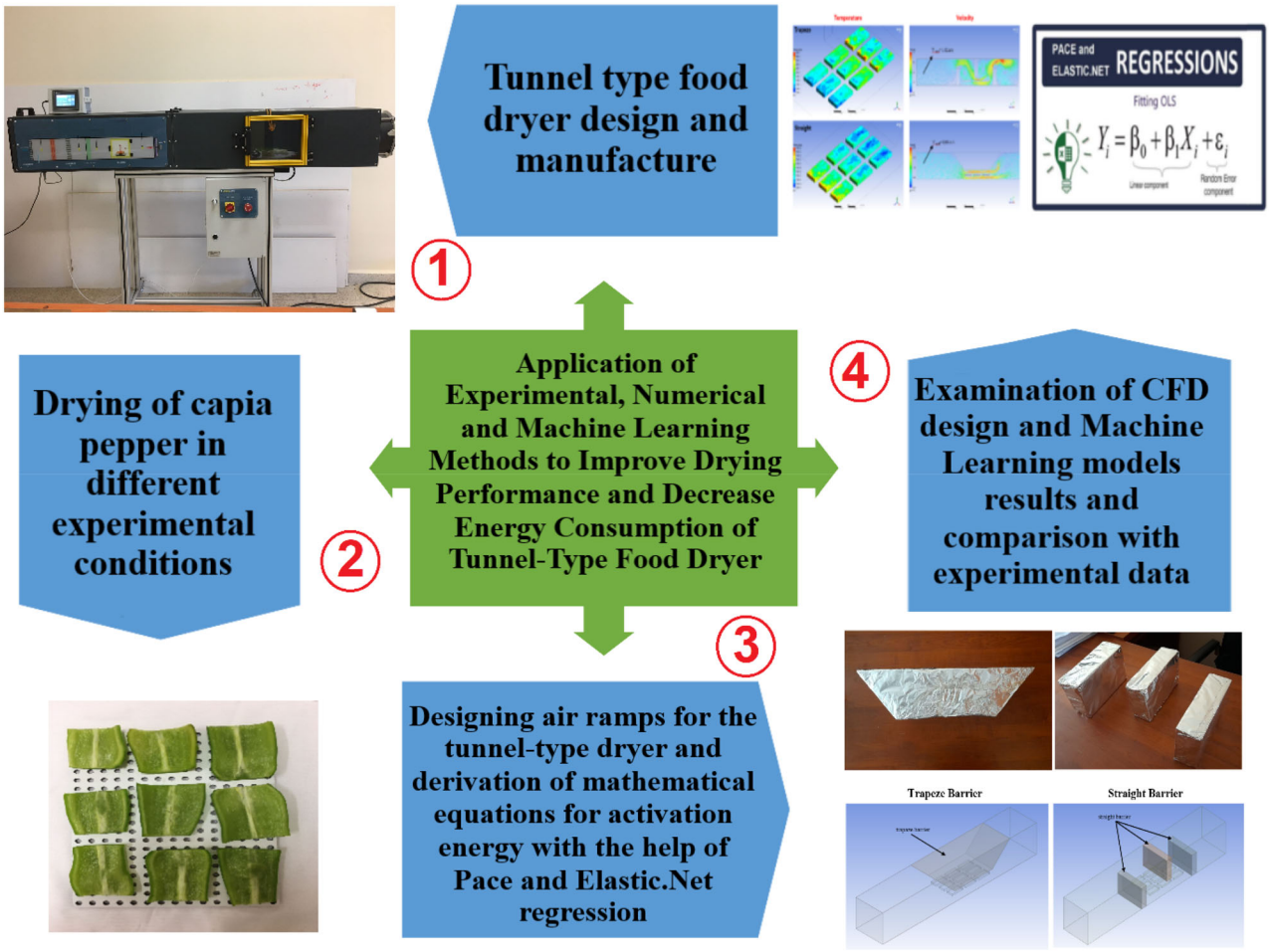

Figure 1. Flowchart of this study.

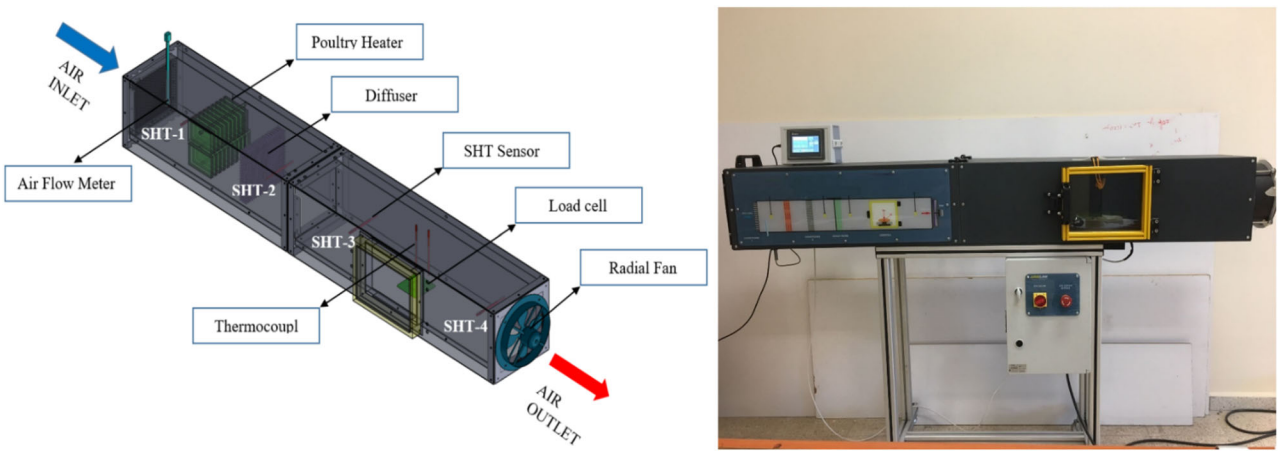

Figure 2. Experimental setup.

leaves the system by passing through the last humidity-temperature sensor (Figure 3).

Straight and trapeze air barriers made of solid and heat-resistant polymer foam were used for Experiment 2, which was conducted to increase the drying chamber performance. The location and dimensions of the air barriers used in the experiments are shown in Figure 4. The air barriers were painted with thermal paint to maintain the adiabatic feature of the drying chamber. It was also covered with thermal foil to prevent surface friction.

In the TTD experiment setup, two inverter drivers adjust the heater power and fan speed, one data logger receives data from the sensors, and a PLC automation

Figure 3. Visuals of the experiments.

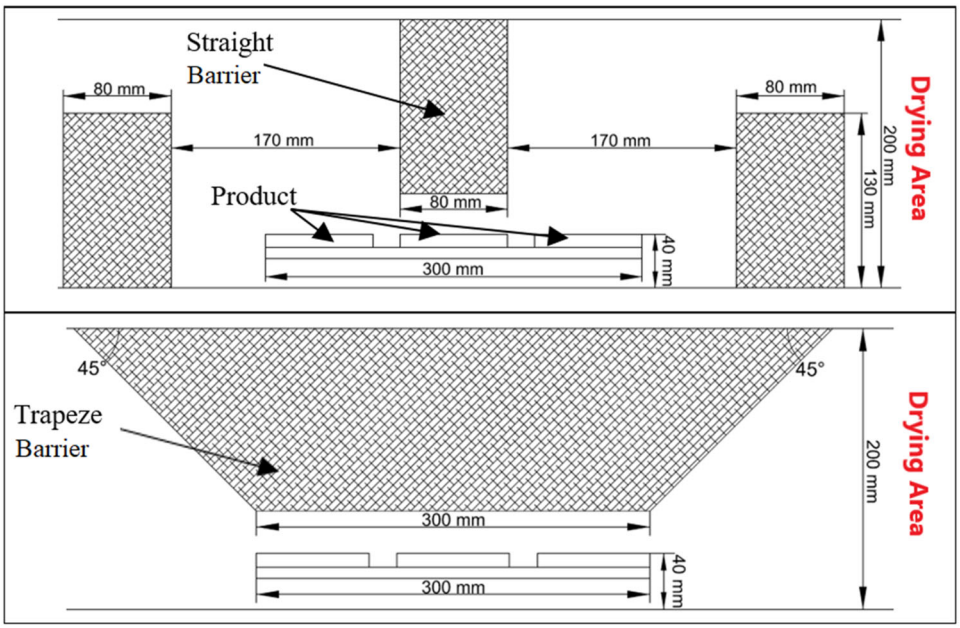

Figure 4. Air barriers.

controls the drying system. The PLC automation flow chart is given in Figure 5.

2.1.1. Experiment 1

A total of three experiments were carried out, two at 50 °C drying air temperature and 1.5 – 1 m/s air speeds, and one at 60 °C and 1.5 m/s air velocity. These experiments aim to obtain a quality mesh structure based on CFD analysis's product surface temperature distribution. In Experiment 1, the existing experimental system dried sliced fresh green peppers weighing 100–105 g and an average size of 80 × 20 mm.

The final moisture of the product was determined with the SHIMADZU MOC-63U moisture analyzer. Figure 6 shows the variation in product surface temperature and product weight during drying. As the product surface temperature increased, the product weight decreased. Experiments were terminated when the change in product weight fell below 1 gram. The final weight of the product was measured as 22 g. The experimental measurement period was determined as every 15 min.

2.1.2. Experiment 2

In Experiment 2, trapeze and straight barriers determined as a result of CFD analysis were placed in the drying chamber, and sliced fresh green peppers weighing 100–105 g and 80 × 20 mm in size were dried. In the experiments, the drying air temperature was kept constant at 50 °C, and the air velocity value was chosen as 1.5 m/s. The experiments were terminated when the weight of the dried product reached 22 g again (Figure 7).

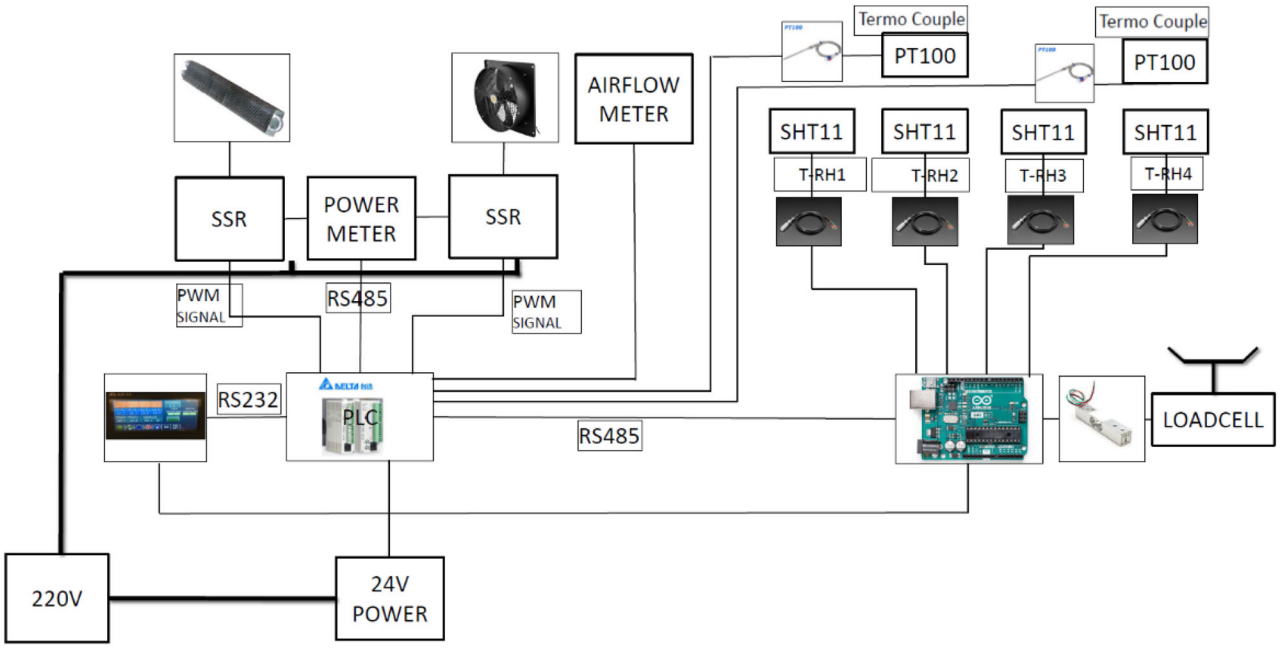

Figure 5. Automation flow chart of TTD experiment system.

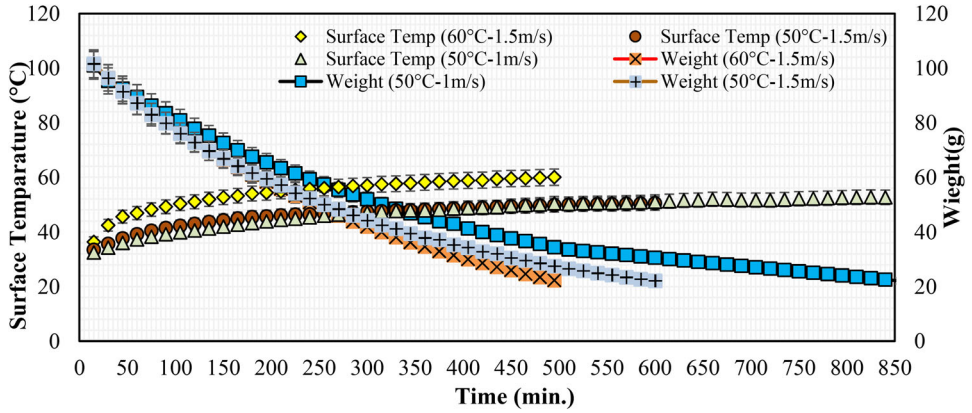

Figure 6. Change in product surface temperature and weight.

2.2. CFD analysis procedure

In this section, ANSYS Fluent program is used to investigate and model the thermal behavior of the designed tunnel dryer. Numerical analyses were performed in the fluent mode for two different purposes. The first is to determine the temperature distribution on the design and product surface, and the second is to observe the behavior of the trapezoidal-flat air barriers on the system performance.

In the first step, the standard design of the TTD (Figure 8a) was created. ANSYS software's design modeler subprogram was used to generate the geometry of the designs to be placed in the TTD dryer chamber. Based on the data obtained in the speed and temperature domain, a modified version of the design was created to achieve better performance (Figure 8b and c).

ANSYS Fluent MESH subroutine is used in the meshing step of TTD. By applying the mesh density test in the design, optimum node, and element sizes are selected to have a reliable solution independent of the mesh size. A mesh density test was performed for the dryer model (without tray) to see the effect of mesh size on product surface temperature. The mesh size has changed from 400000 coarse to 3500000 finer sizes. In Figure 9, as the mesh number increased from 400000 to 2400000, the surface temperature also increased from 314 K to 324 K, and after, and after this point, it was observed that the surface temperature did not change with the increase in the amount of mesh.

The meshes produced for TTD are given in Figure 10. The optimum mesh element sizes for TTDs are 3.448604, 2346395, and 2831566 for standard design, trapezoidal and flat, respectively. In CFD simulations, solutions'

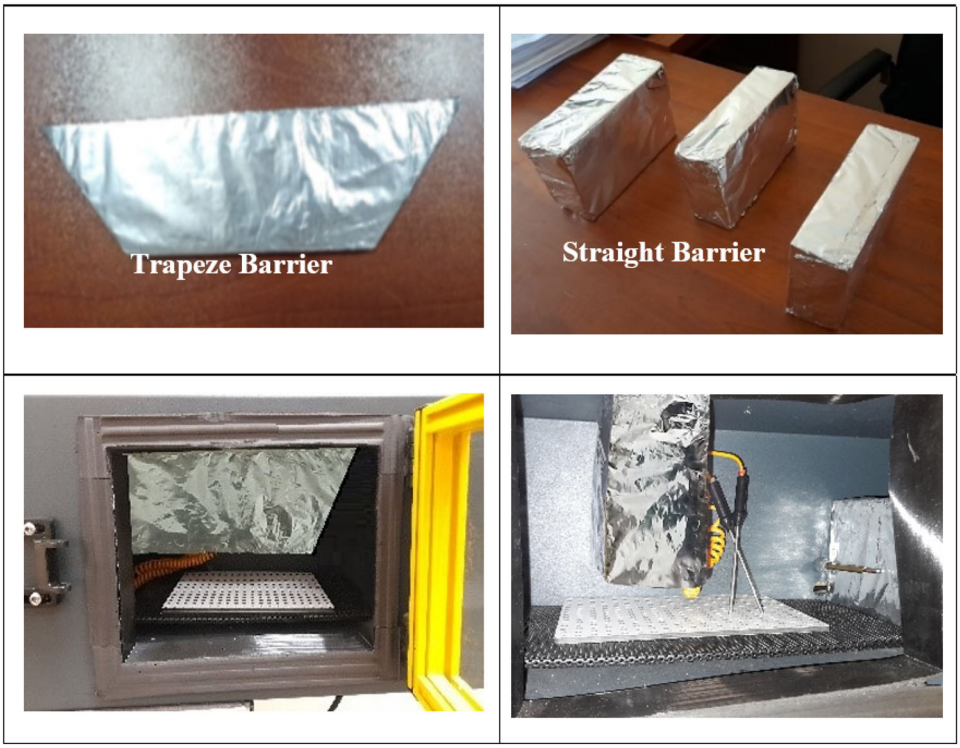

Figure 7. Air barriers for tunnel dryer.

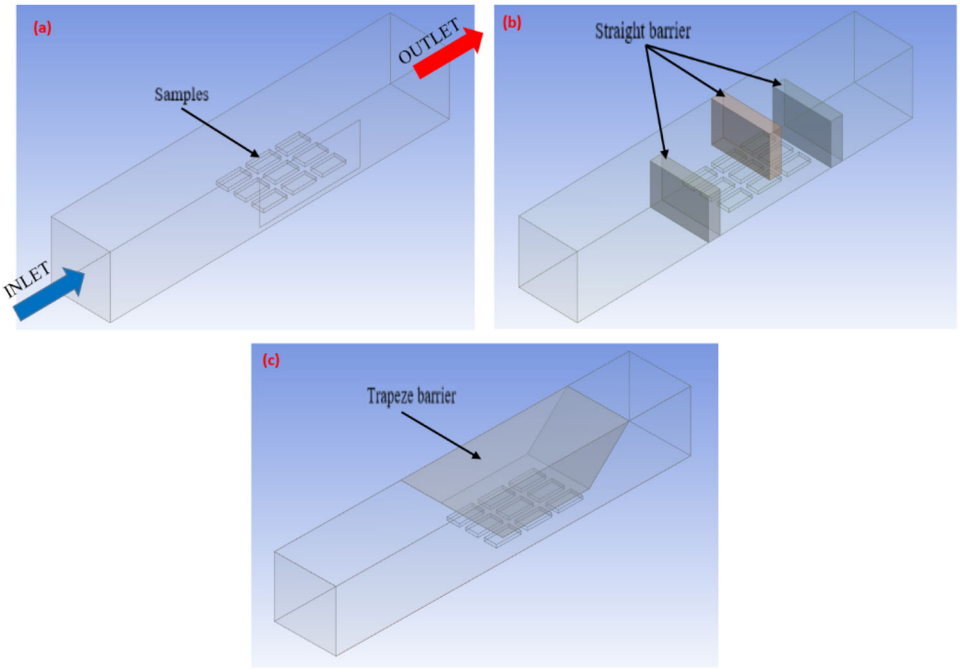

Figure 8. Geometries of standard and modified TTD.

accuracy, fast convergence, and stability depend highly on the mesh quality. Mesh quality is defined by many methods, the most common of which is skewness. In general, skewness; is a function of the angle between any two sides that make up the cell. The skewness value must be below the maximum of 0.95 in CFD studies.[27] The maximum skewness for the lead design, perpendicular and trapeze, is 0.62, 0.63, and 0.53, respectively. In addition, the average skewness value is 0.25, 0.22, and 0.21, respectively, and tetragonal elements are chosen. To refine modeling near the wall and on product surfaces, Mesh was further developed by performing the inflation process consisting of 8 layers (Figure 10a). The net structure created for the analysis was calculated as y^{+} <1 on the

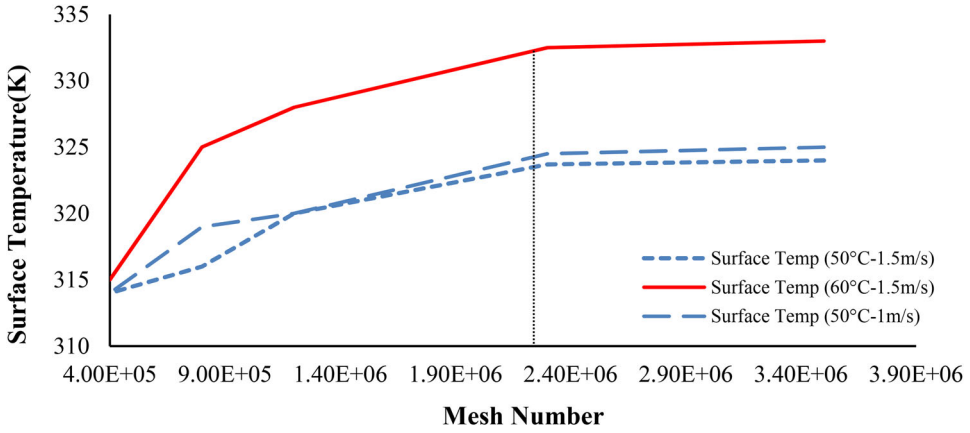

Figure 9. Effect of mesh density on surface temperature for the TDD.

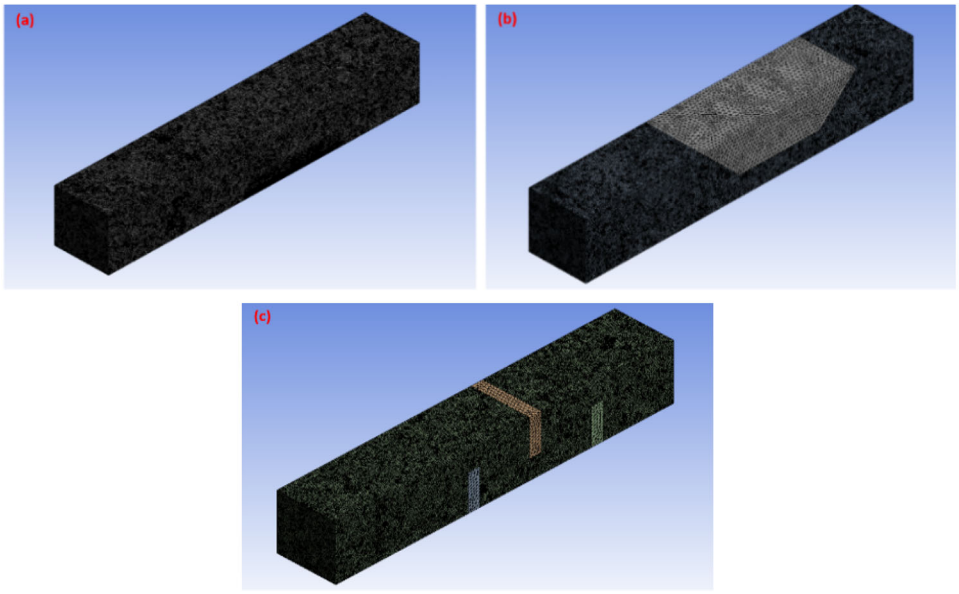

Figure 10. Mesh configurations for TTD: (a) standard design, (b) trapeze, (c) straight.

trapeze wall. Potgieter et al. followed the same method in their work.[28]

Solution equations used in numerical analysis are given in Equations (1)–(6).[29]

Continuity equation:

$$\nabla.\left(\rho.\vec{v}\right) = 0 \tag{1}$$

Navier-Stokes equation:

$$\nabla.\left(\rho.\vec{v}.\vec{v}\right) = -\nabla \mathrm{p} + \nabla.\left(\mu\left[\left(\nabla\vec{v} + \nabla\vec{v}^{T}\right) - \frac{2}{3}\nabla.\vec{v}I\right]\right) \tag{2}$$

Energy equation:

$$\nabla.\left(\vec{\mathrm{V}}\left(\rho\mathrm{E} + \mathrm{p}\right)\right) = \nabla.\left(k_{eff}\nabla\mathrm{T} - \mathrm{h}\vec{\mathrm{J}} + \left(\mu\left[\left(\nabla\vec{v} + \nabla\vec{v}^{T}\right) - \frac{2}{3}\nabla.\vec{v}I\right].\vec{v}\right)\right) + S_h \tag{3}$$

An essential parameter for the energy equation, S_h, refers to the term containing the heat of chemical reaction or other defined volumetric heat sources. The turbulence solver Realizable k-ε equations used in this study are given below in terms of their general form (Equations (4)–(6)).[30]

$$\frac{\partial}{\partial x_j}\left(\rho k u_i\right) = \frac{\partial}{\partial x_{\mathrm{i}}}\left[\left(\mu + \frac{\mu_t}{\sigma_k}\right)\frac{\partial k}{\partial x_i}\right] + G_k + G_b - \rho\varepsilon \tag{4}$$

$$\frac{\partial}{\partial x_i}\left(\rho\varepsilon u_i\right) = \frac{\partial}{\partial x_j}\left[\left(\mu + \frac{\mu_t}{\sigma_\varepsilon}\right)\frac{\partial \varepsilon}{\partial x_i}\right] + \rho C_1 S_\varepsilon - \rho C_2 \frac{\varepsilon^2}{k + \sqrt{\nu\varepsilon}} + C_{1\varepsilon}\frac{\varepsilon}{k}C_{3\varepsilon}G_b \tag{5}$$

$$C_1 = \max\left[0.43, \frac{\eta}{\eta + 5}\right], \rightarrow \eta = S\frac{k}{\varepsilon}, \rightarrow S = \sqrt{2S_{ij}S_{ij}} \tag{6}$$

$$(C_{1\varepsilon} = 1.44),\ (C_2 = 1.9), (\sigma_k = 1.0)(\sigma_\varepsilon = 1.2)$$

Pressure-dependent equations developed by Patankar and Spalding are used as the SIMPLE numerical algorithm. The mass, momentum, and energy equations are iteratively solved for the corresponding boundary conditions using numerical methods until convergence is reached for the relevant variables (velocity, temperature, pressure, and wall heat flux).[31]

2.2.1. Initial and boundary condition

Certain assumptions need to be made to model the experimental conditions numerically. These assumptions facilitate the solution of numerical analysis and express the intervals at which the problem will be solved. The assumptions determined for numerical analysis are defined as initial and boundary conditions.

In this study, the airflow was 3D and entered the dryer at a constant temperature. A mass inlet and an outlet were defined for the dryer. Air distribution at the HGK entrance was the same everywhere. The side surfaces were entirely insulated. Turbulence extinction and turbulent viscosity ratio are 5% and 10%, respectively. The flow in the tunnel is considered incompressible. Analyses are solved by considering steady-state. The boundary condition in the outlet region is defined as the pressure outlet.

2.3. Calculation procedure

In the drying experiments, MC, MR, h_c, and $\square_d$ parameters were examined. The equations used to calculate these parameters are given below.

The amount of moisture in agricultural products is the weight of water retained in the body. The amount of water is defined proportionally in %. Equation (7) was used for the moisture content values of the pepper product according to the dry basis.[4] The moisture rate (MR), which shows the drying process effectively, was calculated with Equation (8).

$$MC_{db} = \frac{W_W}{W_d}100 \tag{7}$$

$$MR = \frac{M_t - M_e}{M_o - M_e} \tag{8}$$

In Equation (8), M_t, M_o, and M_e are the anytime, the initial, and equilibrium moisture contents (% dry basis), respectively.[32]

2.3.1. Determination of the convective heat transfer coefficient (h_c)

The convective heat transfer coefficient (h_c) can be determined using the expression for Nusselt number as[33,34]:

$$h_c = \frac{NuK_V}{X} \qquad h_c = \frac{K_V}{X}\ C(Re.Pr)^n$$

or for forced convection: (9)

The heat utilized for moisture ($\dot{Q}_e$) evaporation is given as[33,34]:

$$\dot{Q}_e = 0.016\frac{K_V}{X}\ C(Re.Pr)^n[P(T_c) - \gamma P(T_e)] \tag{10}$$

On substituting h_c from Equation (9), Equation (10) becomes

$$\dot{Q}_e = 0.016\frac{K_V}{X}\ C(Re.Pr)^n[P(T_c) - \gamma P(T_e)] \tag{11}$$

The moisture evaporated is determined by dividing Equation (11) by the latent heat of vaporization (λ) and multiplying with the area of tray (A_t) and time interval (t)

$$m_e = \frac{\dot{Q}_e}{\lambda}A_t t = 0.016\frac{K_V}{X\lambda}\ C(Re.Pr)^n[P(T_c) - \gamma P(T_e)]A_t t \tag{12}$$

Putting

$$0.016\frac{K_V}{\lambda X}\ [P(T_c) - \gamma P(T_e)]A_t t = Z$$

Equation (13) becomes

$$\frac{m_{ev}}{Z} = \ C(Re.Pr)^n \tag{13}$$

Taking the logarithm of both sides,

$$\ln\left[\frac{m_{ev}}{Z}\right] = \ \ln C + n\ln(Re.Pr) \tag{14}$$

Equation 14 is the analogy of an equation of a straight line,

$$Y = b_1 X + b_0$$

where

$$Y = \ln\left[\frac{m_{ev}}{Z}\right],$$

$b_1 = n,\ X = \ln(Re.Pr)\ b_0 = \ln C,$ thus $C = e^{b_0}$.

The different physical properties of humid air, i.e. density (ρ_v), thermal conductivity (K_v), specific heat (C_v) and viscosity (μ_v), used in the computation of Reynolds number (Re), and Prandtl number (Pr) have been determined using the following polynomial expressions.[33,34] For obtaining physical properties of humid air, T_i is taken as average of product temperature (T_c) and exit air temperature (T_e):

$$\rho_V = \frac{353.44}{(T_i + 273.15)} \quad (15)$$

$$K_V = 0.0244 + 0.6733x10^{-4}T_i \quad (16)$$

$$C_V = 999.2 + 0.1434T_i + 1.101\ x\ 10^{-4}T_i^2 - 6.7581\ x\ 10^{-8}T_i^3 \quad (17)$$

$$\mu_V = 1.718\ x.10^{-5} + 4.620\ x\ 10^{-8}T_i \quad (18)$$

$$P(T) = \exp\left[25.317 - \frac{5144}{(T_i + 273.15)}\right] \quad (19)$$

C and n constant values were determined with the help of linear regression analysis using outlet air temperature, relative humidity value, and evaporative humidity value in the product.

2.3.2. Drying efficiency

The drying efficiency of the tunnel dryer was calculated by considering the power consumption of the fan and heater in the drying system. The ratio of the total amount of energy required to remove moisture from the product to the total energy provided by the drying system refers to the drying efficiency specified in Equation (20).[35] The M_w value in the equation represents the amount of water moving away from the product (kg), the L_h value represents the latent heat of evaporation of water (2381.9 kJ/kg for an average temperature of 50 °C), and the E_{heater} and E_{fan} represent the hourly power consumption (Watt h).

$$\eta d = \frac{Mw \times Lh}{E_{heater} + E_{fan}} \quad (20)$$

2.3.3. Diffusion coefficient and activation energy

The parameter that expresses moisture movement in the product toward the product surface is called effective diffusion (D_{eff}). The D_{eff} parameter can be defined as a function of the product's moisture content and drying time under certain drying conditions. Fick's second law of diffusion is used for determining the D_{eff} coefficient of the product in the drying process. The mathematical expression of this second law developed by Fick and Crank[36] is given in Equation (21).

$$MR = \frac{8}{\pi^2}\exp\left(-\frac{\pi^2 D_{eff} t}{4L^2}\right) \quad (21)$$

In Equation (4), D_{eff} is the effective moisture diffusion in m^2s^{-1}, "t" is time (s), and L is the product half-thickness (m) value. Equation 21 can be written in a logarithmic format as follows.[37,38]

$$\ln(MR) = \ln\left(\frac{8}{\pi^2}\right) - \left(\frac{\pi^2 D_{eff} t}{4L^2}\right) \quad (22)$$

The change of effective diffusivity with temperature is expressed in Equation (23) by Arrhenius equation.[37,38]

$$D_{eff} = D_0 \exp\left(-\frac{E_a}{R(T + 273.15)}\right) \quad (23)$$

In Equation (23), D_0 ($m^2\ s^{-1}$) is the pre-exponential factor of the Arrhenius equation, E_a (kJ/mol) is the activation energy, R (kJ/molK) is the universal gas constant, and T (°C) is the product temperature.

2.4. Uncertainty analyses

Manufacturing, fixed, and random errors have been chosen for the uncertainties that will arise when measuring temperature, air velocity, and humidity parameters. It is necessary to determine the effects of these factors that may create uncertainty on the total measurement uncertainty. Equation (24) calculates the total errors resulting from these effects in the parameters measured in the experiments.[39] In this equation, the total uncertainty is represented by W_R, the measured parameter is symbolized by R, the uncertainties caused by the experimental measurement errors in the tests are shown by x_1, x_2, .., x_n, and the error rates associated with the independent variable are indicated by $w_1, w_2, \ldots, w_n$.

$$W_R = \left[\left(\frac{\delta R}{\delta x_1} w_1\right)^2 + \left(\frac{\delta R}{\delta x_2} w_2\right)^2 + \ldots\ldots\ldots + \left(\frac{\delta R}{\delta x_n} w_n\right)^2\right]^{1/2} \quad (24)$$

2.5. Regression analysis procedure

2.5.1. Pace and Elastic.Net Regression methodology

The regression technique is a famous machine learning algorithm, and it is based on supervised learning that utilizes the independent variable to reach the target value.[22] On the other hand, machine learning consists of generic algorithms that give interesting information about a specific dataset without writing a code.[23]

2.5.2. Pace regression

Pace (Projection Adjustment by Contribution Estimation) regression is an algorithm applied to derive linear models based on analyzing different regression models. Pace regression is used to reveal the model that expresses the relationship between the variable to be modeled and more than one

independent variable.[40] The Pace regression is a machine learning method that produces equations that can express in detail the interaction between the data to be modeled and other parameters in the data set. Pace regression models by blending the ordinary least square, and Empirical Bayes approaches. It generates a mathematical equation to explain the relationship between the modeled parameter and other data in the data set to be created. This equation can be expressed as Equation (25).[41]

$$\text{Modelled Parameter} = \alpha 1\text{Ai} + \alpha 2\text{Bi} + \alpha 3\text{Ci} + \alpha 4\text{Di} + \alpha 5\text{Ei} \tag{25}$$

The weight coefficient αi values affect the parameters obtained by pace regression methods. For the parameters modeled in Equation (18), the input parameters are expressions such as A, B, C, D, and E. It is an important criterion to create linear combinations of features for the model to be obtained. Thus, a simpler modeling design can shorten the required calculation time.

2.5.3. Elastic.Net regression

As the number of data increases, the model created in classical regression analysis becomes more complex. Classical regression analysis is insufficient because assumptions such as multicollinearity, normality, and constant variance are not provided in predictive or classification models.[42] In these cases where the classical regression method is insufficient, the Elastic.Net method, which combines ridge and lasso regression techniques, can be used.[43]

$$\beta(\text{Elastic.Net}) = \arg\min \|y - x\beta\|2 + \lambda_1\|\beta\|2 + \lambda_2\|\beta\| \tag{26}$$

In Equation (26), mixed structure of the ridge and lasso biased estimators are utilized in the calculation procedure. So, λ_1 and λ_2 parameters are the source of estimation in Elastic.Net approach. If $\lambda = 0$, ridge is used as the regression. However, lasso is used when $\lambda = 1$. This parameter is usually taken as 0.5 that is the mean value although it is detected *via* testing in the literature.[44]

Data Set-1 was created using experimental parameters such as product surface temperature, air velocity, drying chamber temperature, drying chamber humidity value, and product weight obtained during the drying process. Data set-1 was obtained from the experiments at 50 °C at 1.5 m/s. Linear mathematical equations were produced for the E_a value using Data Set-1 and Pace and Elastic.Net regression methods. To determine the accuracy of the produced Equations, Data Set-2, created with the parameters obtained from the drying experiments at 60 °C and 1.5 m/s, was used. Five hundred sixty data were used to model the E_a values of drying processes. In machine learning models, 70% of this data was reserved for training and 30% for testing. Machine learning methods were adapted to data sets with MATLAB software. The characteristics of the data used are given in Table 1.

Table 1. Input parameters and output parameters used in machine learning algorithms.

Input parameters				
Parameter	**Notation**	**Unit**	**Min.**	**Max.**
Product temperature	T_{sur}	°C	33.5	50.4
Relative humidity	H	%	16.4	58.15
Product weight	W	g	22.6	101.6
Air speed	V	m/s	1	1.5
Output parameter				
Parameter	**Notation**	**Unit**	**Min.**	**Max.**
Activation energy	E_a	kJ/mol	0.15	0.09

2.5.4. Error analyses

Root mean square error (RMSE) and mean absolute percent error (MAPE) analyses were used to determine the accuracy of the models obtained by Elastic.net and Pace regression methods. In the equations below, A is the actual value, P is the predicted value and n is the number of values.

$$\text{RMSE} = \sqrt{\frac{(P_1 - A_1)^2 + \ldots + (P_n - A_n)^2}{n}} \tag{27}$$

$$\text{MAPE} = \left(\left|\frac{A_n - P_n}{A_n}\right|\right) \cdot 100 \tag{28}$$

3. Result and discussion

This study investigated the drying behaviors of pepper products in a tunnel-type food dryer. A CFD analysis has been applied to speed up the drying process and consume less energy. The results obtained are given below under two headings.

3.1. Calculation procedure results

The calculation procedure was performed for experiments conducted at 50 C temperature and 1.5 m/s air velocity. Experiments were terminated when the change in product weight fell below 1 gram. In the calculation procedure, product weight change, surface temperature, moisture content, drying efficiency, diffusion coefficient values, activation energy, convective heat transfer coefficient, and dimensionless moisture

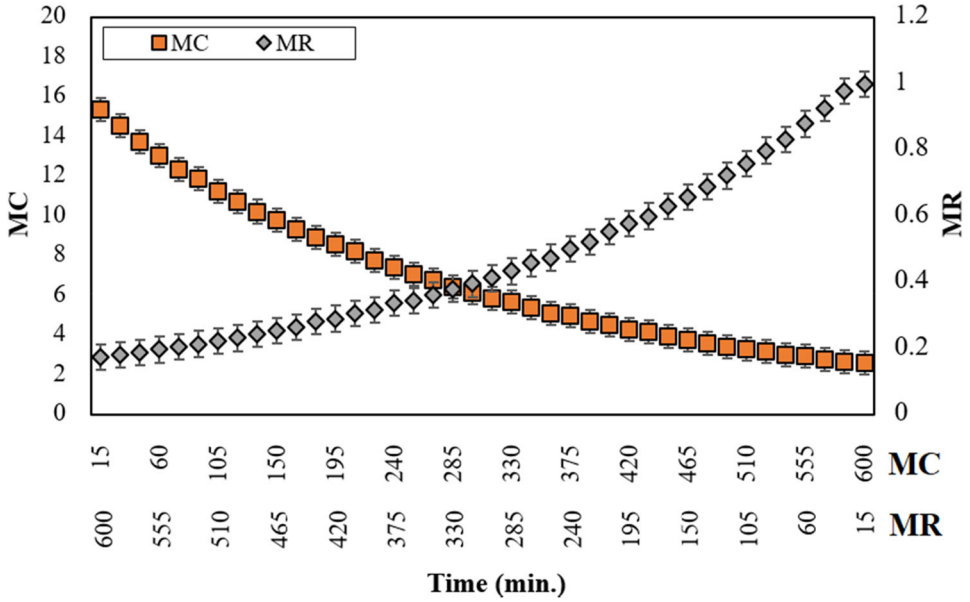

Figure 11. Moisture content and moisture rate variation.

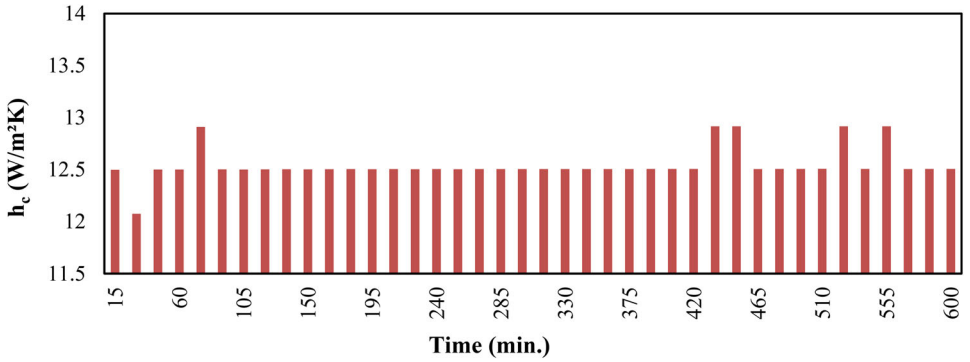

Figure 12. Variation of convective heat transfer coefficient with time.

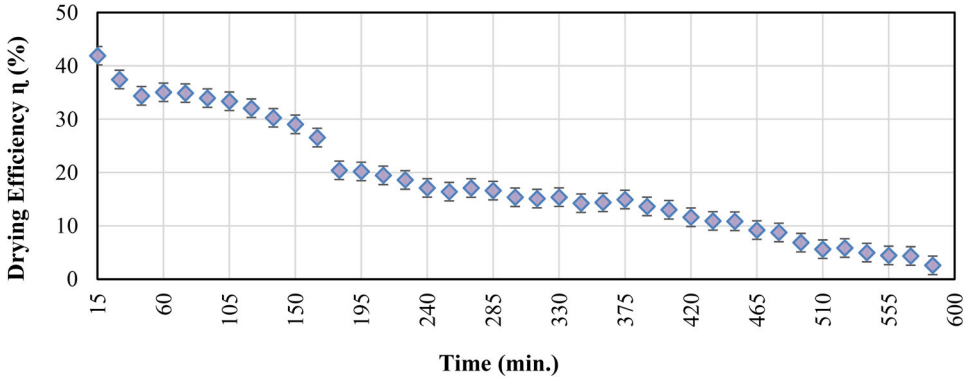

Figure 13. Variation of drying efficiency over time.

ratio values were investigated. The time variation of weight and product surface temperature values measured in all experiments conducted in the tunnel dryer is given in Figure 6.

Figure 11 shows the moisture content and moisture content variation. At the end of the experiment, the product moisture ratio reached 0.174, and the product moisture content got 2.6%. The variation of the convective heat transfer coefficient values between the product's surface and the drying air during the drying period is given in Figure 12. On average, the convective heat transfer coefficient varied between 12.92-12.08 W/m^{2}K.

Figure 13 shows the variation in drying efficiency during the test period. While the average drying

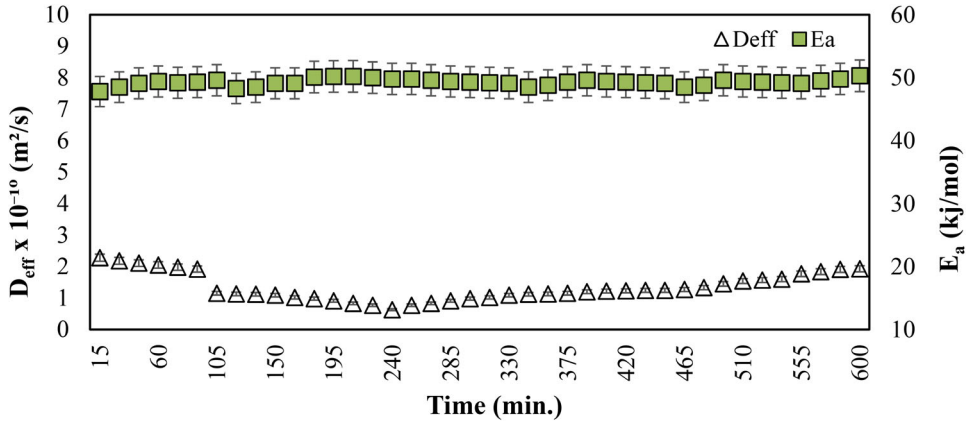

Figure 14. Variation of D_{eff} and E_a values over time.

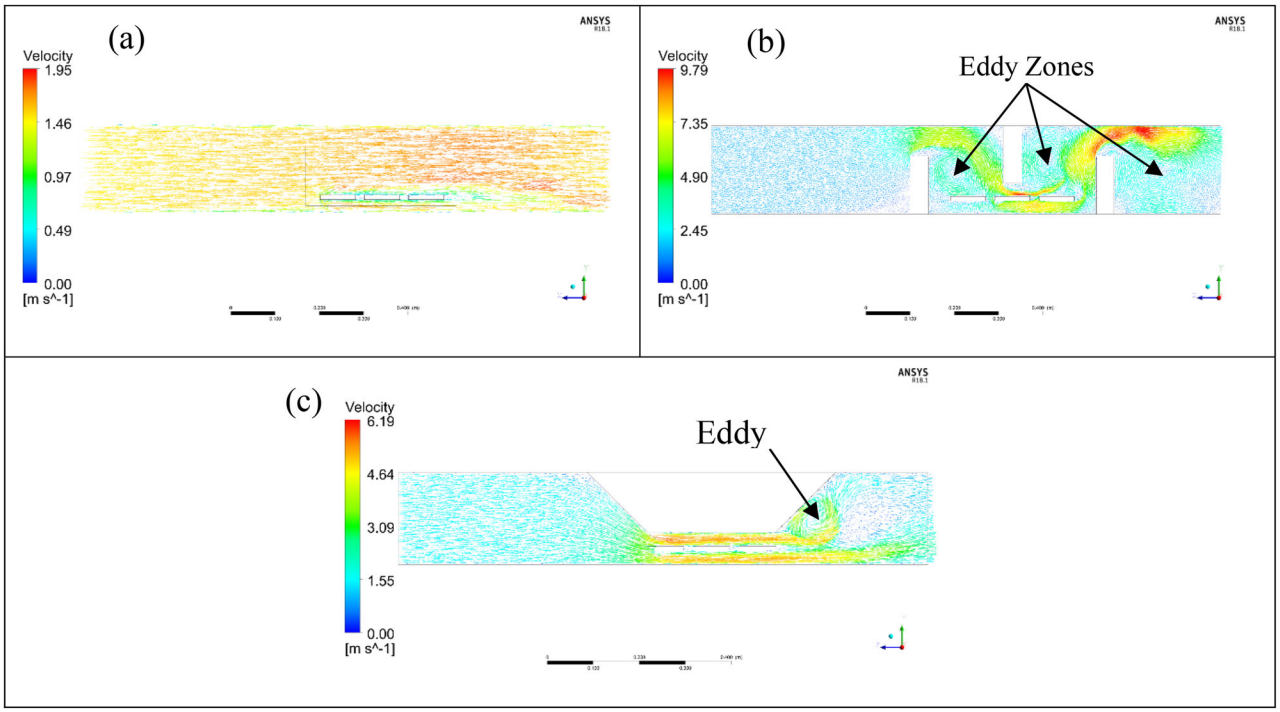

Figure 15. Air velocity distribution: (a) current design, (b) straight barrier design, (c) trapeze barrier design.

efficiency value was 34% during the first 150 min, the average drying efficiency was calculated as 18.4% at the end of the experiment. Since the amount of moisture evaporated from the product in the first period of the drying process is higher, the drying efficiency is high.

In the literature, graphs showing the variation of E_a and D_{eff} parameters according to drying air velocity are generally used.[45] In most studies, these parameters are given as average values.[46] In some studies, graphs expressing E_a and D_{eff} values at the drying process's beginning, middle, and end are added.[47] In this study, the variations of E_a and D_{eff} values according to time during the drying process at 50 C temperature and 1.5 m/s air velocity were given in Figure 14. According to Figure 14, D_{eff} values varied between 2.28×10^{-10} and 0.68×10^{-10} m^2/s, and E_a values ranged between 50.3 and 48.25 kJ/mol.

3.2. CFD simulation results

A full-size greenhouse dryer (Figure 15a) was analyzed in the first step of the simulations. The velocity distribution of the TTD (side view) is shown in Figure 15. As seen in Figure 15a, a homogeneous velocity distribution was obtained around the product in the dryer, and no vortex was observed. Eddy currents were obtained in simulations where air barriers were used to increase the drying performance. Contrary to the trapeze design, the eddy regions are more due to the

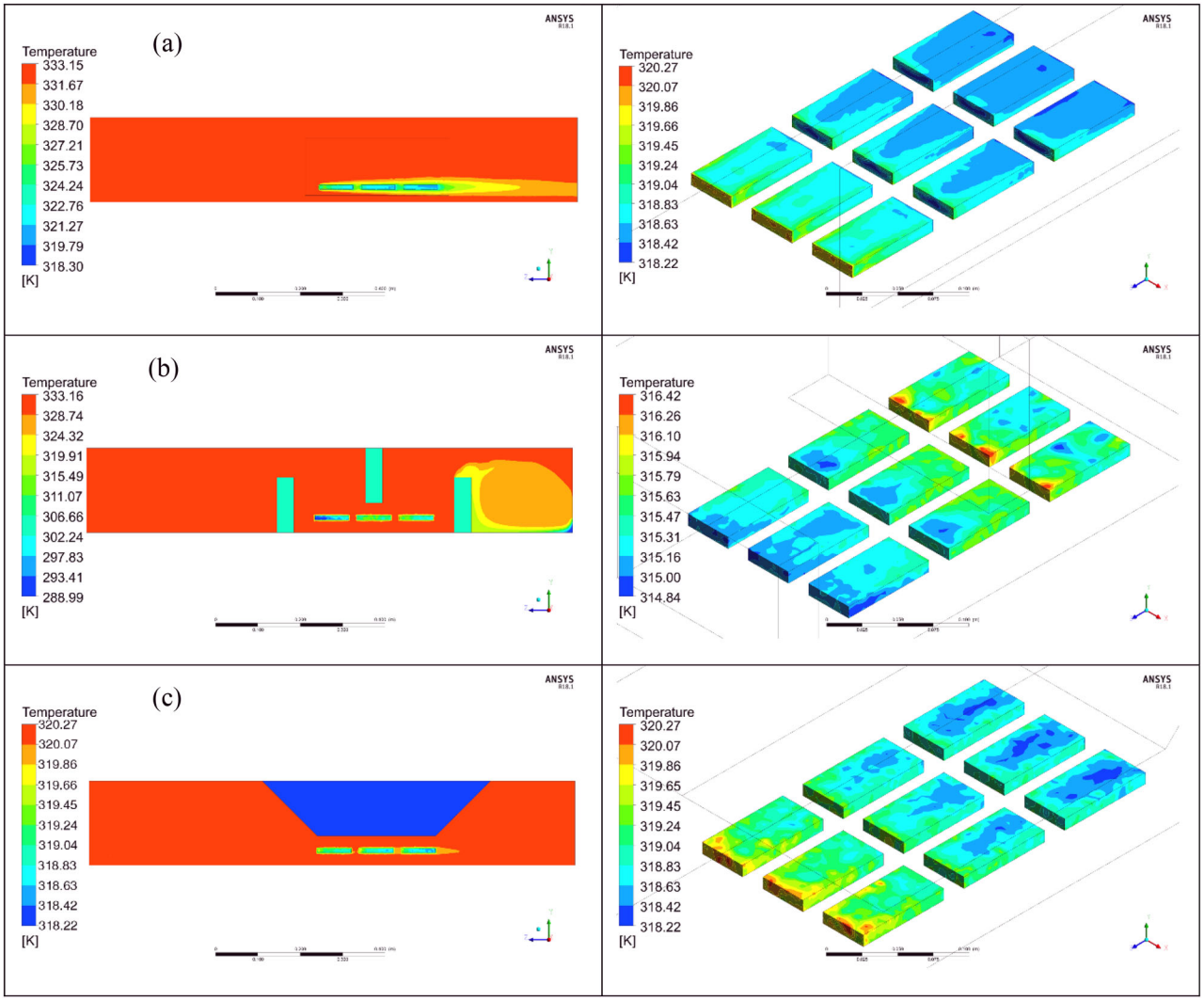

Figure 16. Tunnel-type dryer zone and product surface temperatures distributions: (a) standard design, (b) straight barrier design, (c) trapeze barrier design.

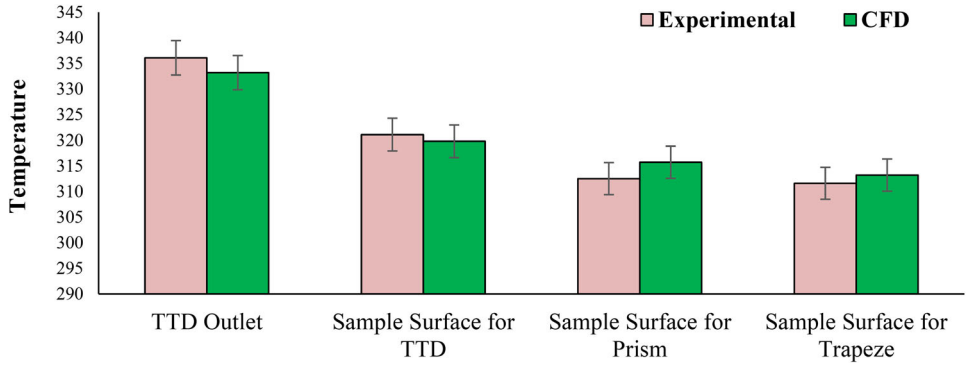

Figure 17. Comparison between CFD and experimental results.

high corner currents in the perpendicular design (Figure 15b and c). These swirl zones have no contribution to the drying process and may cause energy loss. However, the increase in air velocity in these regions will have an effect that reduces the drying time, as it increases the amount of hot air passing over the product. Therefore, in modified designs, it is expected that the trapeze design with less eddy effect will be more effective as it will reduce both energy losses and drying time.

Figure 16 shows the temperature contour in the airspace for three different drying chamber designs.

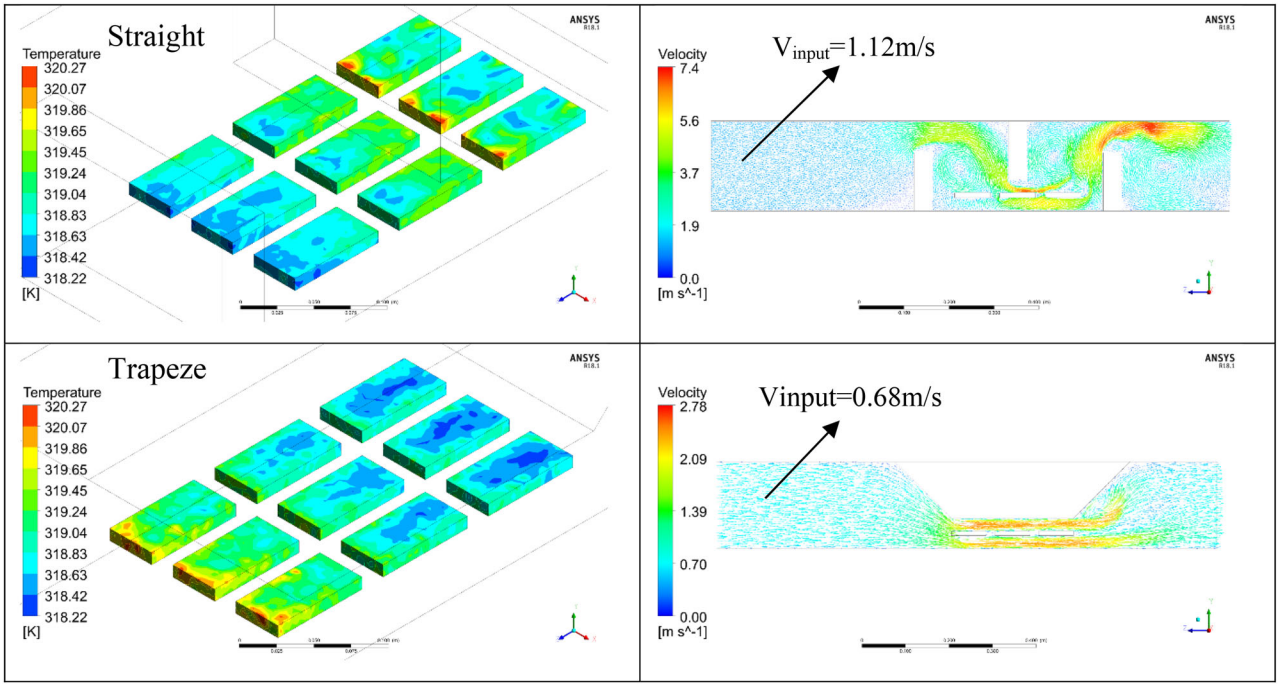

Figure 18. Air velocity distribution for product surface temperatures.

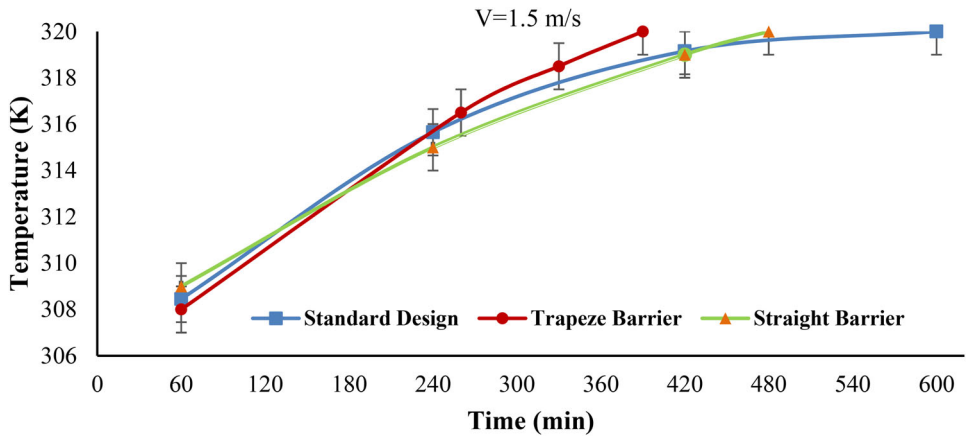

Figure 19. Product surface temperature distribution after trapeze and straight barrier placements.

Since the air velocity distribution is homogeneous in the standard tunnel dryer simulation results, the temperature gradient around the product is also homogeneous. While the ambient temperature was 313.8 K in the standard tunnel dryer, the maximum product surface temperature was 312.5 K. When the air barrier designs placed in the drying chamber were examined under the same experimental conditions, the maximum product surface temperature for the straight barrier was 316.4 K, and the maximum product surface temperature for the trapeze barrier was 320.2 K. This difference in the results is expected because, as can be seen in the velocity distribution (Figure 15), in the trapeze design, since the air passing over the product moves faster, there is an average of 5 K temperature difference from the product surface temperature. Figure 17 shows the product surface temperature values for the drying chamber outlet temperature and the air barriers used, obtained numerically and experimentally. As can be seen, the numerically obtained values are close to the experimental values. The maximum deviation obtained between numerical and experimental temperature values is 8%.

In the CFD simulations results in Figure 18, as a result of the experiments with the standard design, the air velocities that must be given to the system to obtain the product surface temperatures are shown. In Figure 18, to reach the 320 K product surface temperature determined in the standard dryer design, the

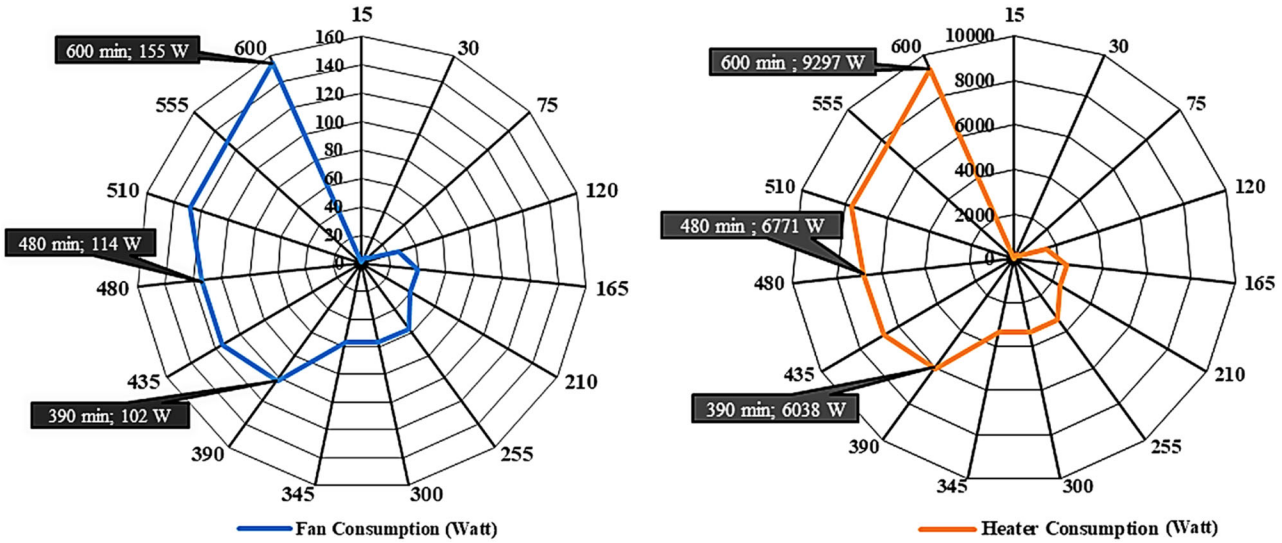

Figure 20. Power consumption to the fan and heater values in the tunnel-type dryer.

Table 2. Efficiency equations obtained with Pace.

Model type	Model equations
Pace	$E_a = 152.0122 + 0.163 * T_{sur} + 0.0005 * W - 3.5111 * H_3 + 1.2731 * H_4 - 1.6505 * T_3 + 0.133 * T_4 + 2.2385 * V$
Elastic.Net	$E_a = 0{,}322 * T_{sur} + 0{,}058 * W - 0{,}141 * H_3 - 0{,}043 * H_4 - 0{,}097 * T_3 + 0{,}098 * T_4 + 0{,}019 * V + 34{,}882$

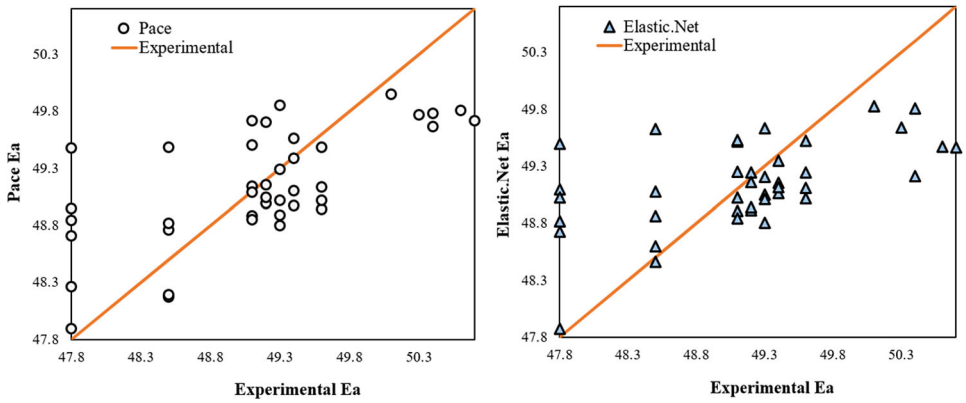

Figure 21. Comparison of Pace and Elastic.Net E_a values with experimental E_a values.

air velocity should be 1.12 m/s in the straight barrier design and 0.68 m/s in the trapeze barrier design. In this case, the air velocity decreased by 24.33% in the straight design and by 54.67% in the trapeze design. The high surface temperature was obtained at low air velocity after the trapeze barrier. Thus, less energy consumption is foreseen.

For the 1.5 m/s air velocity in the standard tunnel design, the experiments, which were terminated according to the test procedure, lasted 600 min, the fan energy consumption was 155 Wh, and the heater energy consumption was 9297 Wh. As a result of the information obtained as a result of the CFD analysis, the repeated experiments with the air barriers took 390 min after the trapeze barrier was placed and 480 min after the straight barrier was placed. This is because, after the trapeze barrier, the air was distributed more evenly and contacted the product surface area more. Thus, thermal losses were reduced, and effective drying was achieved (Figure 19).

The heater and fan consumption values of the tunnel-dryer at 1.5 m/s and 50 °C conditions are given in Figure 20. After 600 min, the electrical energy consumption values of the heater and fan were measured as 9452 Wh in total. The experiments in the straight barrier design under the same conditions took 480 min, and the total energy consumption was 6885 Wh. In the trapeze design, the test period was

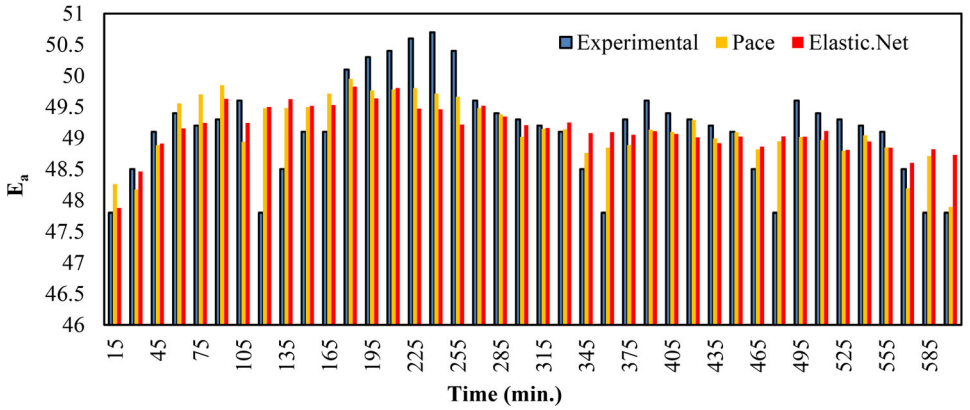

Figure 22. Variation of Pace and Elastic.Net E_a values and experimental E_a values with time.

Table 3. Studies on modeling different drying parameters with machine learning methods.

Modeled parameter	Machine learning method	Error	Reference
Color changes in product	Extreme learning machine-integrated Bayesian methods	0.0563 RMSE	Liu et al. [16]
Shrinkage	Physics Informed Neural Network	0.19 MAPE	Batuwatta-Gamage et al. [17]
D_{eff}	ANFIS	0.074 RMSE	Kaveh et al. [18]
MR	Multiple linear regression	0.6865 RMSE	Meerasri and Sothornvit [19]
MC	Support vector machine	0.033 RMSE	Karaağaç et al. [21]
E_a	ANN	0.02 MAPE	Kartal and Özveren [22]
MR	ANN	0.026 RMSE	Fabani et al. [23]
Residue moisture	Linear regression	0.375 RMSE	Massei et al. [24]
E_a	Pace regression	0.3816 RMSE, 0.0103 MAPE	This work
E_a	Elastic.Net regression	0.2886 RMSE 0.0148 MAPE	This work

390 min, and the total energy consumption was calculated to be 6140 Wh.

3.3. Machine learning models results

In this study, the activation energy of the pepper drying process was calculated in the tunnel-type drying system. E_a values were modeled using Data Set-1, which consists of drying temperature, drying air relative humidity, air velocity, and product weight values obtained from drying experiments. For E_a values, mathematical equations were produced with the help of regression-based artificial intelligence methods Pace and Elastic.Net. E_a equations obtained using Pace, and Elastic.Net methods are shown in Table 2. Data Set-2 obtained from different experimental studies was used to determine the accuracy of the produced equations.

The results of the E_a equations obtained with the experimental values are shown in Figures 21 and 22. The Pace showed similarity to the experimental E_a values with an R^2 value of 0.87. Elastic.net, on the other hand, showed similarity to the experimental E_a values with an R^2 value of 0.93. In Figure 22, the results of the Elastic.net E_a equation approached the experimental E_a values with an RMSE value of 0.2886.

Table 3 shows the machine learning models made for drying parameters in the literature and the results of the models. The table gives model drying parameters, machine learning method, and model error values. The error values of the machine learning models in Table 3 and the Pace and Elastic.net models used in this study are close to each other.

4. Conclusions

The conclusions of this study, which include experimental methods and CFD analysis to increase the product drying rate and reduce the drying energy consumption of a tunnel-type food dryer, are given below.

- The 105 g pepper product drying time in the tunnel dryer was 600 min. During this period, the moisture content of the product decreased from 15.8% to 2.6% and the moisture ratio from 1 to 0.174.
- The convective heat transfer coefficient varied between 12.92 and 12.08 W/m^{2}K during the product drying process.
- The average drying efficiency of the system was calculated as 18.43%.
- With CFD analysis, the effects of the airflow barriers placed in the existing tunnel dryer on drying were examined. The results of these analyses were

compared with the experimental results. CFD analysis results were similar to experimental values with less than 2% error values.

- The drying time was measured as 390 min with trapeze barriers and 480 min with straight barriers. Thus, the trapeze barrier reduced the drying time of the standard design experiment by 45% and the straight barrier by 20%.
- In the tunnel-type drying system, 9.42 kWh of energy was consumed in the product drying process, while this consumption value was measured as 6.14 kWh with the trapeze barrier and 6.88 kWh with the straight barrier. Compared to the standard design, the trapeze barrier design consumed 53.9% less energy, and the straight barrier design consumed 37.2% less energy.
- The mathematical equation produced by pace regression calculated E_a values with an error of 1.03%. Likewise, the mathematical equation produced with Elastic.Net calculated E_a values with an error of 1.48%.

With this study, it has been shown that CFD analysis provides beneficial information before design in tunnel dryers and that significant energy savings can be achieved thanks to the air barrier made within the analyses presented. It is hoped that the methods in this study, which is a reference application to reduce the energy consumption of tunnel-type drying systems, will also be used in different drying systems. In addition, the high calculation success rates of Pace and Elastic.Net E_a equations, validated with different experimental values, show that these machine-learning methods can be used for various parameters in other drying systems.

This study was supported by "Kahramanmaraş Sütçüimam University Scientific Research Foundation" (project number 2021/7-14M). Kahramanmaraş Sütçü Imam Üniversitesi;

References

[1] Zhang, W. P.; Yang, X. H.; Mujumdar, A. S.; Ju, H. Y.; Xiao, H. W. The Influence Mechanism and Control Strategy of Relative Humidity on Hot Air Drying of Fruits and Vegetables: A Review. *Dry. Technol.* **2022**, *40*, 2217–2234. DOI: 10.1080/07373937.2021.1943669.

[2] Matias, G. S.; Lermen, F. H.; Matos, C.; Nicolin, D. J.; Fischer, C.; Rossoni, D. F.; Jorge, L. M. M. A Model of Distributed Parameters for Non-Fickian Diffusion in Grain Drying Based on the Fractional Calculus Approach. *Biosyst. Eng.* **2023**, *226*, 16–26. DOI: 10.1016/j.biosystemseng.2022.12.004.

[3] Daş, M.; Alıç, E.; Kavak Akpinar, E. Numerical and Experimental Analysis of Heat and Mass Transfer in the Drying Process of the Solar Drying System. *Eng. Sci. Technol. Int. J.* **2021**, *24*, 236–246. DOI: 10.1016/j.jestch.2020.10.003.

[4] Das, M.; Alic, E.; Akpinar, E. K. Detailed Analysis of Mass Transfer in Solar Food Dryer with Different Methods. *Int. Commun. Heat Mass Transf.* **2021**, *128*, 105600. DOI: 10.1016/j.icheatmasstransfer.2021.105600.

[5] Barbosa, T. A.; Sousa, J. A.; Arruda, E. B.; Lobato, F. S. Determination of Kinetic and Phenomenological Models to Describe the Guapeva Drying Process in a Tunnel Type Dryer by Using Differential Evolution. *Arab. J. Sci. Eng.* **2022**, *47*, 5693–5703. DOI: 10.1007/s13369-021-05582-y.

[6] Winkel, A.; Mosquera, J.; Aarnink, A. J. A.; Groot Koerkamp, P. W. G.; Ogink, N. W. M. Evaluation of Manure Drying Tunnels to Serve as Dust Filters in the Exhaust of Laying Hen Houses: Emissions of Particulate Matter, Ammonia, and Odour. *Biosyst. Eng.* **2017**, *162*, 81–98. DOI: 10.1016/j.biosystemseng.2017.07.006.

[7] Charmongkolpradit, S.; Somboon, T.; Phatchana, R.; Sang-Aroon, W.; Tanwanichkul, B. Influence of Drying Temperature on Anthocyanin and Moisture Contents in Purple Waxy Corn Kernel Using a Tunnel Dryer. *Case Stud. Therm. Eng.* **2021**, *25*, 100886. DOI: 10.1016/j.csite.2021.100886.

[8] Turgut, S. S.; Küçüköner, E.; Feyissa, A. H.; Karacabey, E. A Novel Drying System – Simultaneous Use of Ohmic Heating with Convectional Air Drying: System Design and Detailed Examination Using CFD. *Innov. Food Sci. Emerg. Technol.* **2021**, *72*, 102727. DOI: 10.1016/j.ifset.2021.102727.

[9] Amanlou, Y.; Zomorodian, A. Applying CFD for Designing a New Fruit Cabinet Dryer. *J. Food Eng.* **2010**, *101*, 8–15. DOI: 10.1016/j.jfoodeng.2010.06.001.

[10] Guangbin, L.; Kaixuan, X.; Qichao, Y.; Yuangyang, Z.; Liansheng, L. Flow Field and Drying Process Analysis of Double-Layer Drying Chamber in Heat Pump Dryer. *Appl. Therm. Eng.* **2022**, *209*, 118261. DOI: 10.1016/j.applthermaleng.2022.118261.

[11] Babu, A. K.; Kumaresan, G.; Antony Aroul Raj, V.; Velraj, R. CFD Studies on Different Configurations of Drying Chamber for Thin-Layer Drying of Leaves. *Energy Sources A Recover. Util. Environ. Eff.* **2020**, *42*, 2227–2239. DOI: 10.1080/15567036.2019.1607935.

[12] Olejnik, T. P.; Mysakowski, T.; Tomtas, P.; Mostowski, R. Optimization of the Beef Drying Process in a Heat Pump Chamber Dryer. *Energies.* **2021**, *14*, 4927. DOI: 10.3390/en14164927.

[13] Darabi, H.; Zomorodian, A.; Akbari, M. H.; Lorestani, A. N. Design a Cabinet Dryer with Two Geometric Configurations Using CFD. *J. Food Sci. Technol.* **2015**, *52*, 359–366. DOI: 10.1007/s13197-013-0983-1.

[14] Razavizadeh, N.; Zare, D.; Nassiri, S. M.; Karim, A.; Eslami, M.; Nematollahi, M. A. Experimental Study

and Numerical Simulation of Resistance to Airflow in a Storage Bin of Rough Rice with Three Inlet Duct Configurations. *Biosyst. Eng.* **2023**, *225*, 118–131. DOI: 10.1016/j.biosystemseng.2022.12.003.

[15] Ju, H. Y.; Vidyarthi, S. K.; Karim, M. A.; Yu, X. L.; Zhang, W. P.; Xiao, H. W. Drying Quality and Energy Consumption Efficient Improvements in Hot Air Drying of Papaya Slices by Step-down Relative Humidity Based on Heat and Mass Transfer Characteristics and 3D Simulation. *Dry. Technol.* **2023**, *41*, 460–476. DOI: 10.1080/07373937.2022.2099416.

[16] Liu, Z. L.; Nan, F.; Zheng, X.; Zielinska, M.; Duan, X.; Deng, L. Z.; Wang, J.; Wu, W.; Gao, Z. J.; Xiao, H. W. Color Prediction of Mushroom Slices during Drying Using Bayesian Extreme Learning Machine. *Dry. Technol.* **2020**, *38*, 1869–1881. DOI: 10.1080/07373937.2019.1675077.

[17] Batuwatta-Gamage, C. P.; Rathnayaka, C. M.; Karunasena, H. C. P.; Wijerathne, W. D. C. C.; Jeong, H.; Welsh, Z. G.; Karim, M. A.; Gu, Y. T. A Physics-Informed Neural Network-Based Surrogate Framework to Predict Moisture Concentration and Shrinkage of a Plant Cell during Drying. *J. Food Eng.* **2022**, *332*, 111137. DOI: 10.1016/j.jfoodeng.2022.111137.

[18] Kaveh, M.; Rasooli Sharabiani, V.; Amiri Chayjan, R.; Taghinezhad, E.; Abbaspour-Gilandeh, Y.; Golpour, I. ANFIS and ANNs Model for Prediction of Moisture Diffusivity and Specific Energy Consumption Potato, Garlic and Cantaloupe Drying under Convective Hot Air Dryer. *Inf. Process. Agric.* **2018**, *5*, 372–387. DOI: 10.1016/j.inpa.2018.05.003.

[19] Meerasri, J.; Sothornvit, R. Artificial Neural Networks (ANNs) and Multiple Linear Regression (MLR) for Prediction of Moisture Content for Coated Pineapple Cubes. *Case Stud. Therm. Eng.* **2022**, *33*, 101942. DOI: 10.1016/j.csite.2022.101942.

[20] Liu, Z. L.; Wei, Z. Y.; Vidyarthi, S. K.; Pan, Z.; Zielinska, M.; Deng, L. Z.; Wang, Q. H.; Wei, Q.; Xiao, H. W. Pulsed Vacuum Drying of Kiwifruit Slices and Drying Process Optimization Based on Artificial Neural Network. *Dry. Technol.* **2021**, *39*, 405–417. DOI: 10.1080/07373937.2020.1817063.

[21] Karaağaç, M. O.; Ergün, A.; Ağbulut, Ü.; Gürel, A. E.; Ceylan, İ. Experimental Analysis of CPV/T Solar Dryer with Nano-Enhanced PCM and Prediction of Drying Parameters Using ANN and SVM Algorithms. *Sol. Energy.* **2021**, *218*, 57–67. DOI: 10.1016/j.solener.2021.02.028.

[22] Kartal, F.; Özveren, U. Prediction of Activation Energy for combustion and Pyrolysis by Means of Machine Learning. *Therm. Sci. Eng. Prog.* **2022**, *33*, 101346. DOI: 10.1016/j.tsep.2022.101346.

[23] Fabani, M. P.; Capossio, J. P.; Román, M. C.; Zhu, W.; Rodriguez, R.; Mazza, G. Producing Non-Traditional Flour from Watermelon Rind Pomace: Artificial Neural Network (ANN) Modeling of the Drying Process. *J. Environ. Manage.* **2021**, *281*, 111915. DOI: 10.1016/j.jenvman.2020.111915.

[24] Massei, A.; Falco, N.; Fissore, D. Use of Machine Learning Tools and NIR Spectra to Estimate Residual Moisture in Freeze-Dried Products. *Spectrochim. Acta A Mol. Biomol. Spectrosc.* **2023**, *293*, 122485. DOI: 10.1016/j.saa.2023.122485.

[25] Liu, Z. L.; Bai, J. W.; Wang, S. X.; Meng, J. S.; Wang, H.; Yu, X. L.; Gao, Z. J.; Xiao, H. W. Prediction of Energy and Exergy of Mushroom Slices Drying in Hot Air Impingement Dryer by Artificial Neural Network. *Dry. Technol.* **2020**, *38*, 1959–1970. DOI: 10.1080/07373937.2019.1607873.

[26] Akay, O. E.; Das, M. Investigation of the Effect of Deposit Layer on Heat Transfer in the Triga Mark-Ii Nuclear Research Reactor Cooling System. *Therm. Sci.* **2022**, *26*, 3987–4001. DOI: 10.2298/TSCI220116065A.

[27] Gilmore, R. C.; Marts, J. A.; Brune, J. F.; Saki, S.; Bogin, G. E.; Grubb, J. W. Simplifying CFD Modeling of Longwall Gobs with a Modular Meshing Approach. *Min. Eng.* **2015**, *67*, 68–72.

[28] Potgieter, M. S. W.; Bester, C. R.; Bhamjee, M. Experimental and CFD Investigation of a Hybrid Solar Air Heater. *Sol. Energy.* **2020**, *195*, 413–428. DOI: 10.1016/j.solener.2019.11.058.

[29] Singh, I.; Vardhan, S.; Singh, S.; Singh, A. Experimental and CFD Analysis of Solar Air Heater Duct Roughened with Multiple Broken Transverse Ribs: A Comparative Study. *Sol. Energy.* **2019**, *188*, 519–532. DOI: 10.1016/j.solener.2019.06.022.

[30] Kumar, D.; Premachandran, B. Effect of Atmospheric Wind on Natural Convection Based Solar Air Heaters. *Int. J. Therm. Sci.* **2019**, *138*, 263–275. DOI: 10.1016/j.ijthermalsci.2018.12.010.

[31] Patankar, S. V.; Spalding, D. B. *A Calculation Procedure for the Transient and Steady-State Behavior of Shell-and-Tube Heat Exchangers*; Heat Exchangers: Design and Theory Sourcebook, 1. McGraw-Hill: New York, 1974.

[32] Doymaz, I. Evaluation of Some Thin-Layer Drying Models of Persimmon Slices (Diospyros kaki L.). *Energy Convers. Manag.* **2012**, *56*, 199–205. DOI: 10.1016/j.enconman.2011.11.027.

[33] Goyal, R. K.; Tiwari, G. N. Heat and Mass Transfer Relations for Crop Drying. *Dry. Technol.* **1998**, *16*, 1741–1754. DOI: 10.1080/07373939808917490.

[34] Jain, D.; Tiwari, G. N. Effect of Greenhouse on Crop Drying under Natural and Forced Convection I: Evaluation of Convective Mass Transfer Coefficient. *Energy Convers. Manag.* **2004**, *45*, 765–783. DOI: 10.1016/S0196-8904(03)00178-X.

[35] Murali, S.; Amulya, P. R.; Alfiya, P. V.; Delfiya, D. S. A.; Samuel, M. P. Design and Performance Evaluation of Solar – LPG Hybrid Dryer for Drying of Shrimps. *Renew. Energy.* **2020**, *147*, 2417–2428. DOI: 10.1016/j.renene.2019.10.002.

[36] Akpinar, E. K. Drying of Mint Leaves in a Solar Dryer and under Open Sun: Modelling, Performance Analyses. *Energy Convers. Manag.* **2010**, *51*, 2407–2418. DOI: 10.1016/j.enconman.2010.05.005.

[37] Crank, J. *The Mathematics of Diffusion*; Clarendon Press: Oxford, **1975**.

[38] Akpinar, E. K.; Toraman, S. Determination of Drying Kinetics and Convective Heat Transfer Coefficients of Ginger Slices. *Heat Mass Transf.* **2016**, *52*, 2271–2281. DOI: 10.1007/s00231-015-1729-6.

[39] Holman, J. P. *Experimental Methods for Engineers*, 8ht ed.; McGraw-Hill: New York, **2012**.

[40] Alic, E.; Das, M.; Kaska, O. Investigation of Nucleate Pool Boiling Heat Transfer by Computational Methods in Different Cylindrical Surfaces and Inclination Angles. Iran. *J. Sci. Technol. Trans. Mech. Eng.* 2023, *47*, 481–495. DOI: 10.1007/s40997-022-00548-3.

[41] Das, M.; Catalkaya, M.; Akay, O. E.; Akpinar, E. K. Impacts of Use PID Control and Artificial Intelligence Methods for Solar Air Heater Energy Performance. *J. Build. Eng.* **2023**, *65*, 105809. DOI: 10.1016/j.jobe.2022.105809.

[42] Ogutu, J. O.; Schulz-Streeck, T.; Piepho, H. P. Genomic Selection Using Regularized Linear Regression Models: Ridge Regression. *BMC Proc.* **2012**, *6*, S10. DOI: 10.1186/1753-6561-6-S2-S10.

[43] Zou, H.; Hastie, T.; Regression, S. Selection via the Elastic Net, with Applications to Microarrays. *J. R. Stat. Soc. Ser. B.* **2005**, *67*, 301–320. DOI: 10.1111/j.1467-9868.2005.00503.x.

[44] Cho, S.; Kim, H.; Oh, S.; Kim, K.; Park, T. Elastic-Net Regularization Approaches for Genome-Wide Association Studies of Rheumatoid Arthritis. *BMC Proc.* **2009**, *3*, 3–8. DOI: 10.1186/1753-6561-3-S7-S25.

[45] Koukouch, A.; Idlimam, A.; Asbik, M.; Sarh, B.; Izrar, B.; Bostyn, S.; Bah, A.; Ansari, O.; Zegaoui, O.; Amine, A. Experimental Determination of the Effective Moisture Diffusivity and Activation Energy during Convective Solar Drying of Olive Pomace Waste. *Renew. Energy.* **2017**, *101*, 565–574. DOI: 10.1016/j.renene.2016.09.006.

[46] Chayjan, R. A.; Salari, K.; Abedi, Q.; Sabziparvar, A. A. Modeling Moisture Diffusivity, Activation Energy and Specific Energy Consumption of Squash Seeds in a Semi Fluidized and Fluidized Bed Drying. *J. Food Sci. Technol.* **2013**, *50*, 667–677. DOI: 10.1007/s13197-011-0399-8.

[47] Kosasih, E. A.; Zikri, A.; Dzaky, M. I. Effects of Drying Temperature, Airflow, and Cut Segment on Drying Rate and Activation Energy of Elephant Cassava. *Case Stud. Therm. Eng.* **2020**, *19*, 100633. DOI: 10.1016/j.csite.2020.100633.